RSC Advances

PAPER

View Article Online
View Journal | View Issue

Cite this: *RSC Adv.*, 2025, **15**, 17023

A photothermal energy storage phase change material with high stability and enthalpy†

Shenghua Xiong,*[ab] Yanlong Shi,[ab] Changhui Liu[ab] and Yunyun Yang *[ab]

Received 27th February 2025
Accepted 13th May 2025

DOI: 10.1039/d5ra01422k

rsc.li/rsc-advances

In this study, CNT-BN-SA-1 composites were prepared by vacuum impregnation using stearic acid (SA) as a phase change material (PCM), multi-walled carbon nanotubes (CNT) and hexagonal boron nitride (BN) as support materials. According to the results of the thermal conductivity of CNT-BN-SA-1, the maximum thermal conductivity of CNT-BN-SA-1 is 0.83 W m K^{-1} when the CNT-BN content reaches 15 wt%. The surface morphology, heat storage capacity, and reliability of CNT-BN-SA-1 were systematically studied. The melting temperature (ΔT_m) of CNT-BN-SA-1 is 51.83 °C and the latent calorific value is 143.5 ± 5.0 J g^{-1}. CNT-BN-SA-1 still exhibits good latent heat capacity after 1000 heat treatment cycles, and its latent heat after cycling is 147.3 ± 5.0 J g^{-1}. After a high temperature of 100 °C, CNT-BN-SA-1 still retains a good solid shape. The results show that CNT-BN-SA-1 has high latent heat, reliability, and excellent CSP energy storage capabilities. It has great application potential in the field of FSPCMs. This method provides a certain reference for the preparation of phase change composites.

1. Introduction

In recent years, the growth rate of energy demand and carbon emissions has reached an unprecedented level.[1,2] As a renewable energy source, solar power holds significant strategic importance for meeting long-term energy needs, owing to its advantages such as abundant reserves and reliability.[3] Currently, the storage forms of sun solar energy mainly include photothermal,[4–6] photoelectric,[7,8] and thermochemical energy conversion,[9,10] of which photothermal conversion was one of the rapidly developing solar energy utilization methods in recent years. Therefore, fully harnessing solar energy stands as one of the optimal solutions to address the issue of energy scarcity.[11,12] Scholars both domestically and internationally have conducted extensive theoretical research and practical applications aimed at enhancing the efficiency of solar energy and fossil fuels.[13–15] Among them, the use of phase change energy storage technology has been proven to be an effective measure.[16–18] Phase change energy storage technologies in the fields of solar energy, geothermal energy, and buildings have been widely used.[19–22] This technology leverages the characteristic of phase change materials to absorb or release a substantial amount of latent heat during the phase transition process, thereby achieving the release and storage of energy.[23–25] Based on their chemical composition, phase change materials are categorized into three types: organic, inorganic, and composite phase change materials.[26] Organic phase change materials have the advantages of being non-corrosive, non-toxic, eutectic, good chemical stability, *etc.*[27,28] And it can provide a wide range of operating temperatures. Wei *et al.*[29] prepared the phase change material C_{22}-CMFP microcapsulated phase change material by *in situ* polymerization, which had a high enthalpy value and thermal stability, and its enthalpy value reached 205.7 J g^{-1} and did not leak after 12 h at 100 °C. Ding *et al.*[30] extracted lignocellulosic nanoparticles (LCNPs) from bovine feces by a simple filtration and centrifugation method, and then prepared phase change material (PCM) microcapsules with melamine formaldehyde shells using LCNP-stabilized Pickering emulsions as templates. The obtained PCM microcapsules have good thermal stability and durability, with a PCM core content of up to 88.9% and a phase change enthalpy of 214.3 J g^{-1}, which is expected to be used in thermal energy storage and temperature regulation applications. Mo *et al.*[31] developed a Ti_3C_2Tx@PVA/PEG composite material with high thermal conductivity (0.428 W (m^{-1} K^{-1})), high phase change enthalpy (131.1 J g^{-1}), excellent photothermal conversion efficiency (96.5%), and structural stability, making it suitable for thermal energy management. Chen *et al.*[32] prepared MXene@PVP/PEG composite PCM (MPP) with high latent heat (140.5 J g^{-1}), excellent shape stability, 96.2% photothermal conversion efficiency, and good cycling stability, making it suitable for solar energy conversion and thermal storage. The research on these outstanding phase change materials has opened up new perspectives and directions for the study of phase change composites.

However, the previous organic phase change material packaging technology has a complex operation process, long

[a]*College of Civil Aviation Safety Engineering, Civil Aviation Flight University of China, Guanghan 618307, China. E-mail: yunyun1990@cafuc.edu.cn; xsh@my.swjtu.edu.cn*
[b]*Civil Aircraft Fire Science and Safety Engineering Key Laboratory of Sichuan Province, Civil Aviation Flight University of China, Guanghan 618307, China*

† Electronic supplementary information (ESI) available. See DOI: https://doi.org/10.1039/d5ra01422k

preparation cycle, low packaging efficiency, and low atomic utilization rate,[33] which significantly increases the production cost. The latent heat of the resulting product is relatively low, which greatly reduces the efficiency of solar energy utilization. Therefore, employing encapsulation and porous adsorption techniques to maintain the stable form of phase change materials (FSPCMs), prevent leakage, and enhance their thermal conductivity is crucial for the development of solar energy.[34,35] For example, Zhang[36] prepared PA-SA (palmitic-stearic acid)/expanded graphite composite materials by melting-mixing physical blending method. The phase transition temperature and latent heat of prepared samples were about 54 °C and 166 J g^{-1}, respectively. The material maintained good storage/release characteristics after 720 accelerated thermal cycling tests, demonstrating the excellent thermal reliability of prepared samples. Yang *et al.*[37] prepared a series of phase change composites by electrostatic self-assembly using carboxylated WCNT and h-BN as raw materials. The latent heat of the composite is 188 J g^{-1} and remains stable after 1000 cycles. However, due to the poor interface interaction of some SA encapsulation materials, the stability and reliability of the prepared FSPCMs have been poor. The support material cannot maintain a long service life of SA under the action of external forces, chemicals, and thermal radiation. Therefore, most researchers create stable and reliable FSPCM by enhancing the interaction of PCM with support materials.[38–40]

In this paper, the solid–liquid phase change materials CNT-SA and CNT-NB-SA were prepared by modifying MWCNT or h-BN carboxylationation, and self-assembling the carboxyl-containing SA under the drive of hydrogen bonds. CNT-BN prevents SA from leaking due to external action, improving the durability of FSPCM. In addition, the chemical structure, crystal properties, thermal stability, phase transformation properties and thermal reliability of CNT-SA and CNT-BN-SA were characterized. The results show that CNT-BN has the function of photothermal conversion, which provides a good control strategy for the preparation of phase change materials.

2. Experiment materials and methods

2.1 Materials

Stearic acid (SA, CAS: 57-11-4), *N*-(3-dimethyl aminopropyl)-*N*′-ethyl carbodiimide hydrochloride (EDC. HCl, CAS: 7084-11-9), *N*,*N*-dimethylformamide (DMF, CAS: 68-12-2) was provided by Chengdu Cologne Chemical Co., Ltd, China. Hexagonal boron nitride nanoparticles were obtained by Shanghai Titan Technology Co., Ltd, China (h-BN, CAS: 10043-11-5 size = 5–10 μm). Multi-walled carbon nanotubes were purchased from Chengdu Organic Chemical Co., Ltd, China (MWCNTs, φ = 30–50 nm, Φ = 50–60 nm, length = 5–30 μm, specific surface area = 120 m^2 g^{-1}). MWCNTs were carboxylated with a mixture of concentrated sulfuric acid and nitric acid (mass ratio = 3 : 1),[41] and the carboxylated sample was named CNT-BN (with the ratio-to-mass ratio of BN nanosheets to CNTs is 1 : 1 and 1 : 2).[37]

2.2 Preparation of FSPCM

FSPCMs were prepared using a vacuum impregnation system, as shown in Fig. 1. For SA samples, SA is melted in a flask at 100 °C and then poured into a PTFE dish where it is cooled and crystallized to form a round SA sample. For CNT-SA samples, the CNT is heated in an Erlenmeyer flask to 100 °C and then the molten SA is poured into it under vacuum. After cooling, CNT-SA (mass ratio of CNT = 15%) is obtained. A certain amount of BN nanosheets and CNT were added to 50 mL of DMF in a certain proportion to disperse evenly by ultrasonication, and then 100 mg HOBt, 100 mg EDC· HCl, 1.187 g DIPEA, stirred vigorously for 48 h, to obtain CNT-BN composites (mass ratios of CNT and BN were 1 : 1 and 1 : 2, respectively), and then the precipitate was filtered, washed and lyophilized to obtain CNT-BN hybrid nanosheets. Then, two FSPCMs with CNT-BN as support materials were prepared, the mass fraction of CNT-BN was 15%, and when the mass ratio of BN to CNT was 1 : 1, the sample was named CNT-BN-SA-1. When the mass ratio of BN to CNT is 2 : 1, the sample is named CNT-BN-SA-2.

2.3 Characterizations and performance evaluation

The chemical structure of CNT, BN, SA, and FSPCMs was characterized by Fourier transform infrared spectrophotometer (Nicolet-560, Nicolet Co, USA) in attenuated total reflection mode. Test temperature: room temperature (25 °C), wavenumber range 400–4000 cm^{-1} and resolution 4 cm^{-1}. Thermogravimetric analysis (TGA) of CNT-SA, CNT-BN-SA-1, and CNT-BN-SA-2 was performed under an N_2 atmosphere using a thermogravimetric analyzer (TGA4000, PE, USA). Its heating rate is 10 K min^{-1}, and the temperature range was 30–600 °C. The crystallization properties of CNT and CNT-BN-SA-1 were studied by X-ray diffraction (XRD). Its temperature range was 5–50 °C, scanning rate 0.04° min^{-1}, and temperature 25 °C. The phase transition temperature and latent heat of CNT-SA, CNT-BN-A-1, and CNT-BN-SA-2 at heating or cooling rates of 10 K min^{-1} were determined by differential scanning calorimetry (DSC Q200). The masses of the measured samples were 3–5 mg. The sample was first heated to avoid the effects of the thermal properties of the

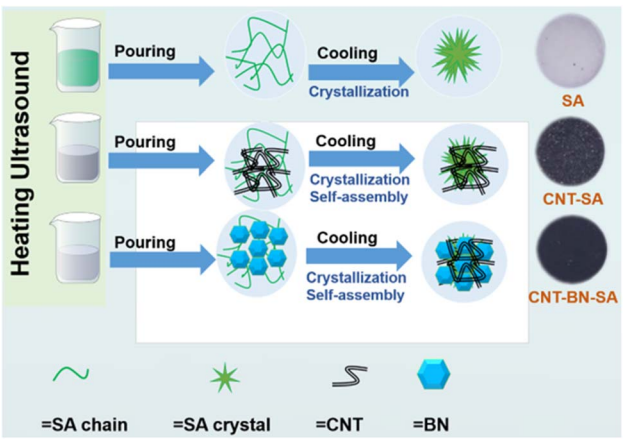

Fig. 1 Preparation process of SA, CNT-SA, and CNT-BN-SA.

previous processing of the sample, and then the sample was cooled to obtain DSC cooling data. Further heating measured DSC heating performance. Samples are heated and cooled at a heating rate of 3 K min^{-1} in the temperature range of 25–80 °C and repeated 1000 or 500 times in a temperature-controlled chamber. These repetitive tests were designed to accelerate thermal cycling testing. These processed samples were named CNT-SA-1k, CNT-BN-SA-1-1k, and CNT-BN-SA-2-1k. The accelerating voltage was set to 5.0 kV, and the micromorphological characteristics of CNT-BN-SA-1 and CNT-SA were observed by field emission scanning electron microscopy (FESEM, Nova NanoSEM450, Thermo Fisher Scientific, USA).

3. Results and discussions

3.1 Infrared and thermogravimetric analysis

The FT-IR of FTIR spectra for SA, carboxylated CNT, uncarboxylated CNT, carboxylated BN, uncarboxylated BN, and CNT-BN-SA-1 are shown in Fig. 2a. As can be seen from the figure, the carboxylated CNT has an obvious expansion and contraction vibration peak at 1540 cm^{-1}, which is the result of the strengthening of the carboxyl group here. The FT-IR of carboxylated BN and non-carboxylated BN remained basically unchanged. The apparent absorption peak of SA is changed due to the electrostatic self-assembly effect of the carboxylated CNT and the carboxyl groups of BN and SA driven by hydrogen bonding. It can also be seen from the figure that after electrostatic self-assembly, there is C–H at 3000 cm^{-1} in CNT-BN-SA-1 and a –COOH carboxyl group at 1684 cm^{-1}. The thermal degradation peaks shift (Table S1†) and degradation curves of FSPCMs were shown in Fig. 2b and c, indicating that electrostatic self-installation hinders the volatilization of SA to some extent. As shown in Fig. 2, XPS characterization of CNT-BN-SA-1 was performed by XPS on d, e, and f. A peak at 289.16 eV attributing to the C=O bond, as shown in Fig. 2d. In addition, the peaks belonging to C–N and N–O were found in the N1s spectrum to be 399.56 eV and 398.01 eV, respectively, as shown in Fig. 2e. The peaks of 532.16 eV and 533.59 eV in the spectrum of O1s is attributed to the C=O and C–O bonds, as shown in Fig. 2f. The appearance and disappearance of peaks in X-ray photoelectron spectroscopy and infrared testing suggest that phase change materials have carboxylic acid groups.

3.2. Crystallization properties and thermal conductivity

As shown in Fig. 3a, 15 wt% CNT and BN increase the thermal conductivity of SA by 256% ~266%. CNT-BN-SA-1 has high thermal conductivity, with a thermal conductivity of 0.83 W m K^{-1}. Fig. 3 shows the XRD characterization of CNT-BN, SA, and CNT-BN-SA-1. It can be seen from the figure that SA and CNT-BN-SA-1 have obvious diffraction peaks at 22.6°, indicating that they have excellent crystallization properties, and their diffraction peaks do not change significantly, indicating that CNT-BN does not affect the crystallization properties of SA.

3.3 Phase change behavior

DSC is a method for determining the energy storage capacity of a material and the phase change temperature. The DSC curves of CNT-SA, CNT-BN-SA-1, and CNT-BN-SA-2 and the corresponding DSC curves after 1000 times of heating and cooling, as well as the histogram of phase transition characteristics, are shown in Fig. 4. Table 2 of the ESI† shows the phase transition temperature and enthalpy values of SA, CNT-SA, CNT-BN-SA-1,

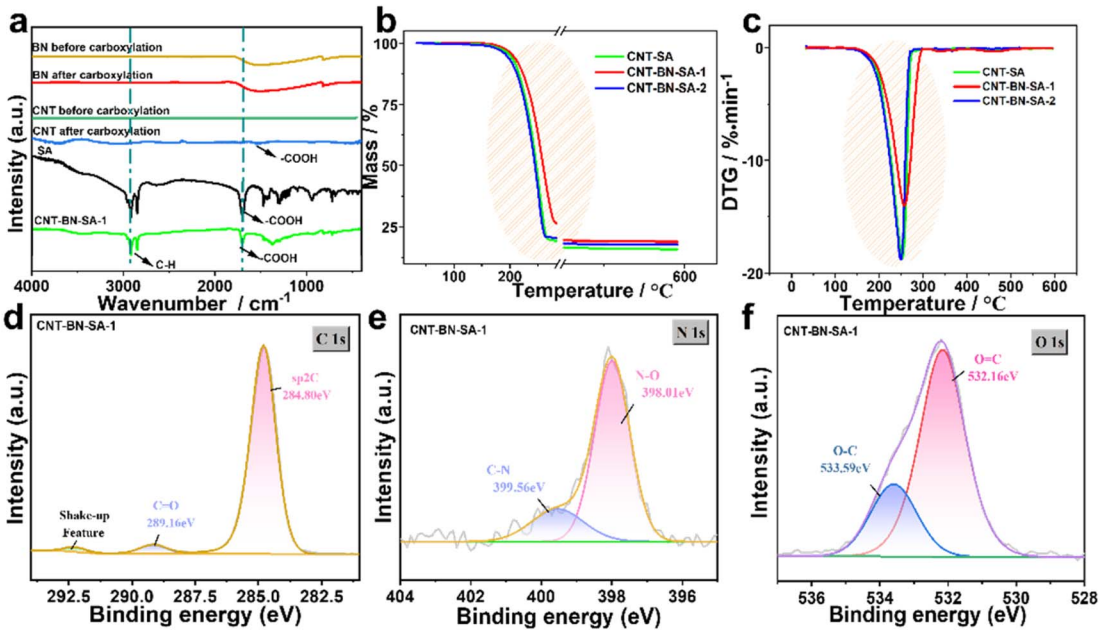

Fig. 2 (a) FTIR spectra of SA, carboxylated CNT, non-carboxylated CNT, carboxylated BN, uncarboxylated BN, and CNT-BN-SA-1. (b) The TG curves of CNT-SA, CNT-BN-SA-1, and CNT-BN-SA-2 (c) the DTG curves of CNT-SA, CNT-BN-SA-1and CNT-BN-SA-2. XPS test chart of CNT-BN-SA-1. (d) C1s. (e) N1s. (f) O1s.

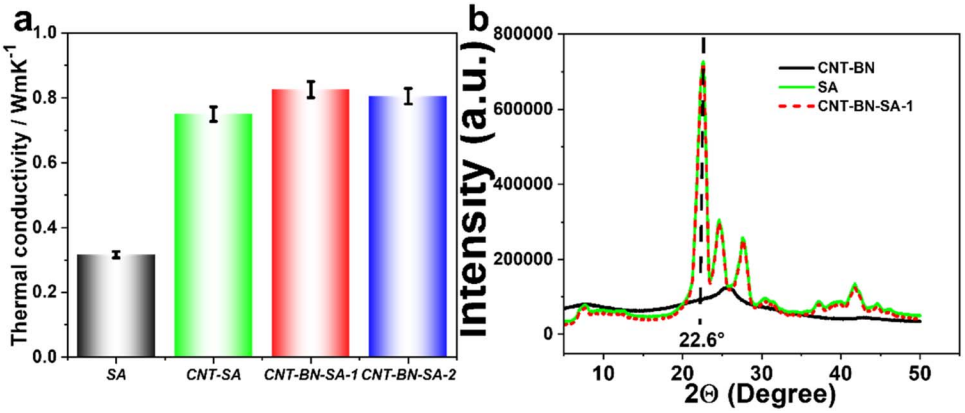

Fig. 3 (a) the thermal conductivity of SA, CNT-SA, CNT-BN-SA-1, and CNT-BN-SA-2 (b) the XRD diffractogram of CNT-BN, SA and CNT-BN-SA-1.

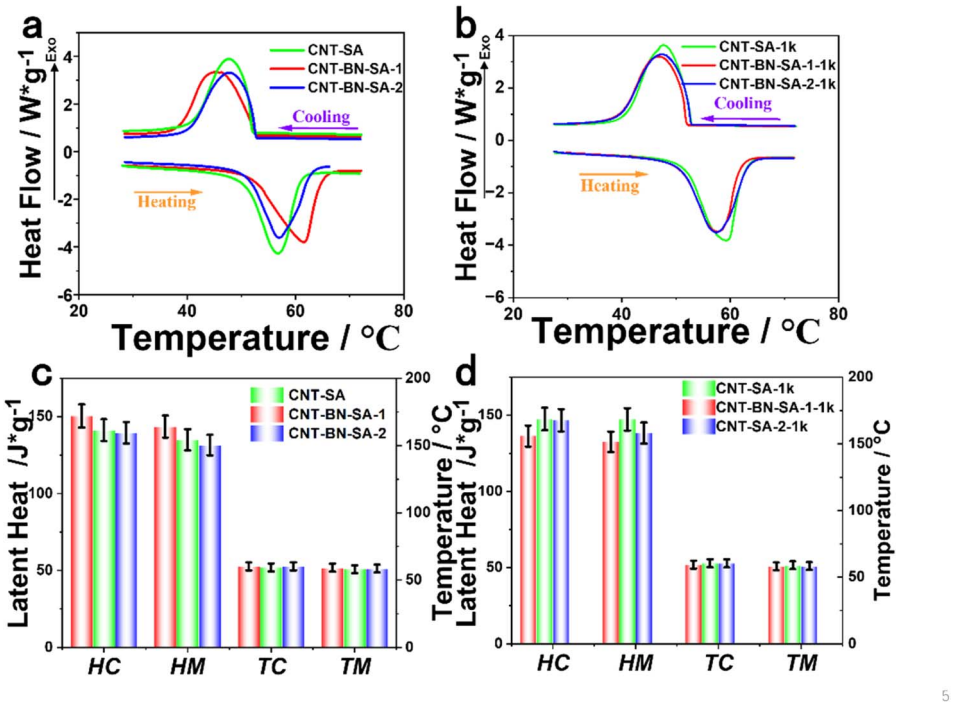

Fig. 4 (a) DSC curves for CNT-SA, CNT-BN-SA-1, and CNT-BN-SA-2. (b) DSC curves of CNT-SA, CNT-BN-SA-1, and CNT-BN-SA-2 after 1000 heating–cooling cycles. (c) Phase transition characteristics of CNT-SA, CNT-BN-SA-1, and CNT-BN-SA-2 (d) phase change characteristics of CNT-SA-1k, CNT-BN-SA-1-1k, and CNT-BN-SA-2-1k (1000 cycles after heating and cooling).

and CNT-BN-SA-2. As can be seen from Fig. 4c, the ΔH_m of CNT-SA is 135.0 ± 5.0 J g^{-1}. The ΔH_m of CNT-BN-SA-1 was 143.5 ± 5.0 J g^{-1}. ΔH_m 131.6 ± 5.0±5.0 J g^{-1} of CNT-BN-SA-2. Compared with CNT-SA, the latent heat and phase transition temperature of CNT-BN-SA-1 after 1000 heat treatment cycles changed slightly, and the ΔH_m was 147.3 ± 5.0 J g^{-1}, this is due to the improved crystallization properties of SA after the cycle test., as shown in Fig. 4d. In contrast, the ΔH_m of CNT-SA decreases after 1000 cycles, which is due to SA leakage after 1000 cycles, which further indicates that the addition of BN is beneficial for improving the stability of the sample. The results show that CNT-BN-SA-1 has high latent heat and good thermal stability. It has certain reference significance in the preparation of phase change materials. In addition, Table 1 compares the latent heat and loading capacity of the CNT-BN-SA developed in this study with stearic acid in other PCMs. It is worth noting that the CNT-BN-SA composite has a suitable high latent heat and a load capacity of up to 51.8%, which is somewhat competitive compared to other studies.

3.4 Photothermal and high-temperature resistance

Thermal leakage at 20 °C, 50 °C, and 100 °C for SA and FSPCM, respectively, as shown in Fig. 5a. As the temperature increases,

Table 1 The latent heats and comparisons of different PCMs

PCM	Carrying capacity (%)	Latent heats (J/g^{-1})	Reference
Stearic acid/expanded graphite	38.9	163.5	42
Stearic acid/expanded graphite composites	45.0	140.4	43
Stearic acid/carbonized maize straw composite	49.5	160.7	44
Stearic acid/Carbon nanotubes	51.8	147.3	This work

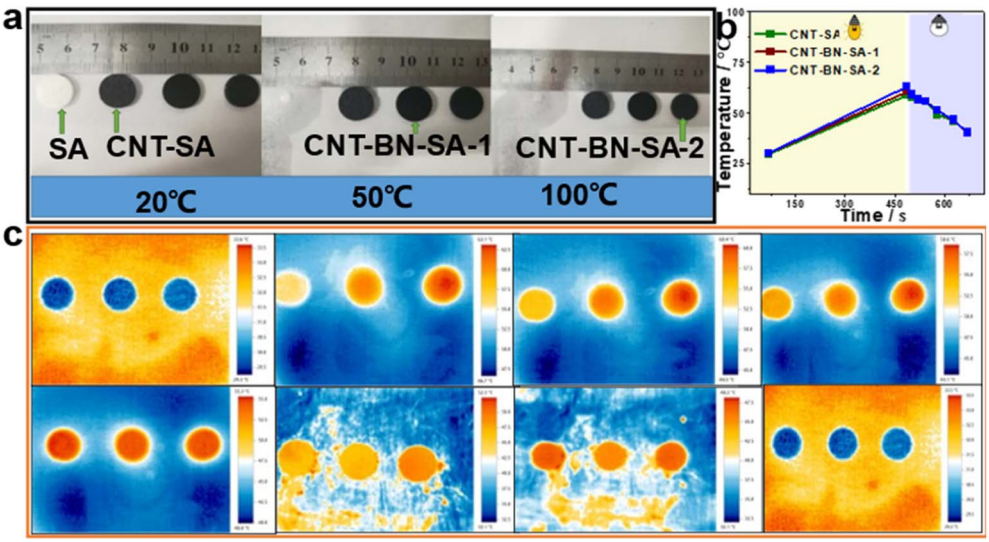

Fig. 5 (a) SA, CNT-SA, CNT-BN-SA-1, and CNT-BN-SA-2 photographs of infrared light irradiation at 20 °C, 50 °C and 100 °C, respectively (b) photothermal temperature curves of CNT-SA, CNT-BN-SA-1 and CNT-BN-SA-2 under infrared light on and off for 50–650 s (c) the real-time photos of CNT-SA, CNT-BN-SA-1 and CNT-BN-SA-2 from left to right.

the SA gradually melts, while the FSPCM remains solid at 100 °C. The photothermal properties of the FSPCM were tested using testo 883 and the temperature curve over time is shown in Fig. 5b. The temperatures of CNT-SA, CNT-BN-SA-1, and CNT-BN-SA-2 reached a maximum of 58.8 °C, 60.5 °C and 63.1 °C, respectively, when infrared light was irradiated at room temperature of 22 °C for 487 s. When the IR lamp is turned off, the CNT-SA, CNT-BN-SA-1, and CNT-BN-SA-2 temperatures

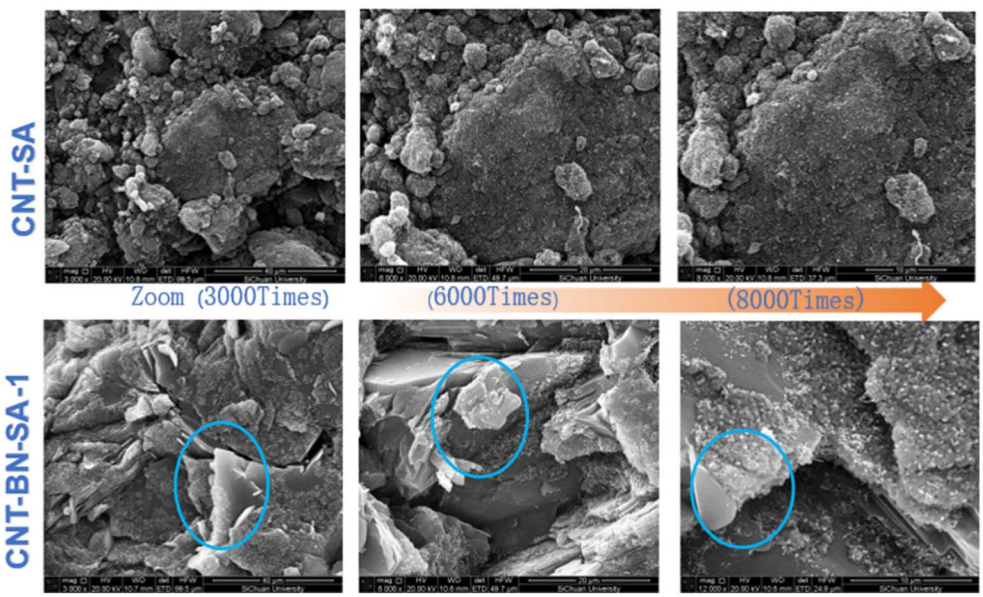

Fig. 6 The SEM images of CNT-SA and CNT-BN-SA-1 zoom in 3000 times, 6000 times, and 8000 times.

decrease slowly, and after 182 s, the temperatures of CNT-SA, CNT-BN-SA-1, and CNT-BN-SA-2 are still above 40 °C. Fig. 5c shows the real-time photos of CNT-SA, CNT-BN-SA-1, and CNT-BN-SA-2 from left to right, from left to right, representing the real-time temperature at 8 o'clock in Fig. 5b, and the second image reaches the maximum temperature, and then turns off the IR lamp to test the cooling process. This temperature retention is attributed to the effective photon capture capacity of the CNT and CNT-BN, which achieves a photothermal efficiency of 52.4%, calculated as shown in Table 3 of the ESI.† It can be concluded that CNT and CNT-BN have good encapsulation effects on SA leakage, and CNT-BN-SA-1 has good photothermal and energy storage functions, calculated as shown in Table 4 of the ESI.†.

3.5 Surface topography

Further SEM characterization of CNT-SA and CNT-BN-SA-2 was performed. Fig. 6 shows the surface micromorphology of CNT-SA and CNT-BN-SA-1. The surface of CNT-SA was very rough and homogeneous spherical, while the surface of CNT-BN-SA-1 was tightly connected in layers. This was due to the presence of the dispersion BN (about 10–20 μm) in the FSPCM composite. The fine distribution of CNT and CNT-BN shows that electrostatic self-assembly CNT and CNT-BN provide a certain control strategy for the uniform dispersion of PCMs in the carrier material in the future.

4. Conclusions

In this study, we prepared CNT-BN-SA-1, a photothermal phase change energy storage material with excellent stability, long life, and high enthalpy value. The △Hm of CNT-BN-SA-1 is 143.5 ± 5.0 J g^{-1}, which has the desired high enthalpy value. Then, CNT-BN-SA-1 was heat treated 1000 times, and the ΔH_m of the samples was 147.3 ± 5.0 J g^{-1}, showing good thermal reliability. CNT-BN-SA-1 was placed under the infrared lamp, and the surface was rapidly increased from room temperature 25 °C to 64.1 °C. When the infrared lamp is removed, the temperature of CNT-BN-SA-1 is kept above 40 °C for 182 s, showing good photothermal and heat storage capacity. The preparation method of high enthalpy and high stability phase change materials can provide some guidance for the uniform dispersion of phase change materials in the carrier materials. Due to insufficient mechanical properties, the application of CNT-BN-SA-1 is limited. In the future, it is necessary to develop composite phase change materials that possess both high phase change enthalpy and strong mechanical properties as a breakthrough direction. Through multi-scale structural design and interface reinforcement, it is possible to achieve simultaneous optimization of thermal storage performance and mechanical performance.

Data availability

The datasets used during the current study are available from the corresponding author (Yunyun Yang: yunyun1990@cafuc.edu.cn) upon reasonable request.

Author contributions

S. X. conceived the writing and preparation of PU materials, Y. S. and C. L. analyzed the results, and Y. Y. supported the construction. All authors reviewed the manuscript and revision.

Conflicts of interest

The authors declare no competing financial interest.

Acknowledgements

This work was financially supported by the National Key R&D Program of China (No. 2024YFC3014400), the National Natural Science Foundation of China (No. 52403077), the Sichuan Science and Technology Program (No. 2025ZNSFSC0146), the Opening Foundation of Civil Aircraft Fire Science and Safety Engineering Key Laboratory of Sichuan Province (No. MZ2024KF05).

References

1 P. A. Raymond, J. Hartmann, R. Lauerwald, S. Sobek, C. McDonald, M. Hoover, D. Butman, R. Striegl, E. Mayorga, C. Humborg, P. Kortelainen, H. Durr, M. Meybeck, P. Ciais and P. Guth, Global carbon dioxide emissions from inland waters, *Nature*, 2013, **503**, 355–359.
2 C. Liu, Y. Xu, Y. Shi, Z. Jiang, P. Wang, J. Wei and Y. Yang, Research and Application Progress of Photo-Induced Self-healing Polymers, *Mater. Today Commun.*, 2025, 111752.
3 W. Kong, Y. Yang, A. Yuan, L. Jiang, X. Fu, Y. Wang, H. Xu, Z. Liu and J. Lei, Processable and recyclable crosslinking solid-solid phase change materials based on dynamic disulfide covalent adaptable networks for thermal energy storage, *Energy*, 2021, **232**, 121070.
4 Y. Wang, B. Tang and S. Zhang, Single-walled carbon nanotube/phase change material composites: sunlight-driven, reversible, form-stable phase transitions for solar thermal energy storage, *Adv. Funct. Mater.*, 2013, **23**, 4354–4360.
5 C. Tian, Y. Yang, Q. Liu, Y. Bai, F. Zhao, L. Huang, N. Yang, X. Cai and W. Kong, Molecular Regulation of Flexible Composite Solid–Solid Phase Change Materials with Controllable Isotropic Thermal Conductivity for Thermal Energy Storage, *ACS Appl. Mater. Interfaces*, 2023, **15**, 13165–13175.
6 Y. Yang, C. Liu, Y. Shi, P. Wang, Y. Xu and W. Kong, Intrinsic photothermal block polyurethane solid–solid phase-change materials with high mechanical toughness and multi-recyclability controlled by crosslinking density, *J. Energy Storage*, 2025, **113**, 115583.
7 R. Rawat, R. Lamba and S. Kaushik, Thermodynamic study of solar photovoltaic energy conversion: An overview, *Renewable Sustainable Energy Rev.*, 2017, **71**, 630–638.
8 M. Yu, Y. Qu, K. Pan, G. Wang and Y. Li, Enhanced photoelectric conversion efficiency of dye-sensitized solar

cells by the synergetic effect of $NaYF_4$: Er3+/Yb3+ and g-C_3N_4, *Sci. China Mater.*, 2017, **3**, 228–238.

9 X. Peng, T. W. Root and C. T. Maravelias, Storing solar energy with chemistry: the role of thermochemical storage in concentrating solar power, *Green Chem.*, 2017, **19**, 2427–2438.

10 Y. Yang, B. Liu, T. Zhang, Y. Wu, P. Wang, C. Liu, Y. Shi and S. Mu, Improved design, analysis, preparation and properties of photothermal phase-change polyurethane materials based on zinc ion coordination, *Prog. Org. Coat.*, 2025, **201**, 109098.

11 A. Kasaeian, F. Rajaee and W.-M. Yan, Osmotic desalination by solar energy: A critical review, *Renewable Energy*, 2019, **134**, 1473–1490.

12 Y. Yang, W. Kong and X. Cai, Synthesis and characterization of comb-like crosslinking polyurethane based form-stable phase-change materials for thermal energy storage, *Polym. Adv. Technol.*, 2021, **32**, 4162–4170.

13 O. Gencel, A. Yaras, G. Hekimoğlu, A. Ustaoglu, E. Erdogmus, M. Sutcu and A. Sarı, Cement based-thermal energy storage mortar including blast furnace slag/capric acid shape-stabilized phase change material: Physical, mechanical, thermal properties and solar thermoregulation performance, *Energy Build.*, 2022, **258**, 111849.

14 D. P. Hanak and V. Manovic, Linking renewables and fossil fuels with carbon capture via energy storage for a sustainable energy future, *Front. Chem. Sci. Eng.*, 2020, **14**, 453–459.

15 M. Huo, Z. Wu, T. He and D. Li, Thermodynamic modeling and control of hybrid solar-fossil fuel power generation and storage system, *Appl. Therm. Eng.*, 2023, **229**, 120593.

16 D. Zhang, C. Li, N. Lin, B. Xie and J. Chen, Enhanced properties of mica-based composite phase change materials for thermal energy storage, *J. Energy Storage*, 2021, **42**, 103106.

17 K. Wang, T. Yan, L. Meng and W. Pan, A Review on Microencapsulated Phase-Change Materials: Preparation, Photothermal Conversion Performance, Energy Storage, and Application, *Sol. RRL*, 2023, **7**, 2300447.

18 R. Bai, S. Liu, J. Han, M. Wang, W. Gao, D. Wu and M. Zhou, Expanded vermiculite supported capric–palmitic acid composites for thermal energy storage, *RSC Adv.*, 2023, **13**, 17516–17525.

19 V. Tyagi, K. Chopra, R. Sharma, A. Pandey, S. Tyagi, M. S. Ahmad, A. Sarı and R. Kothari, A comprehensive review on phase change materials for heat storage applications: Development, characterization, thermal and chemical stability, *Sol. Energy Mater. Sol. Cells*, 2022, **234**, 111392.

20 V. Tyagi, K. Chopra, B. Kalidasan, A. Chauhan, U. Stritih, S. Anand, A. Pandey, A. Sarı and R. Kothari, Phase change material based advance solar thermal energy storage systems for building heating and cooling applications: A prospective research approach, *Sustain. Energy Technol. Assessments*, 2021, **47**, 101318.

21 G. Hekimoğlu, M. Nas, M. Ouikhalfan, A. Sarı, V. Tyagi, R. Sharma, Ş. Kurbetci and T. A. Saleh, Silica fume/capric acid-stearic acid PCM included-cementitious composite for thermal controlling of buildings: Thermal energy storage and mechanical properties, *Energy*, 2021, **219**, 119588.

22 G. Hekimoğlu, M. Nas, M. Ouikhalfan, A. Sarı, Ş. Kurbetci, V. Tyagi, R. Sharma and T. A. Saleh, Thermal management performance and mechanical properties of a novel cementitious composite containing fly ash/lauric acid-myristic acid as form-stable phase change material, *Constr. Build. Mater.*, 2021, **274**, 122105.

23 B. Xie, C. Li and Y.-L. He, Advanced electro-heat conversion properties of microcrystalline graphite-based composite phase change material with the three-dimensional framework, *J. Energy Storage*, 2023, **59**, 106367.

24 M. Terhan and G. Ilgar, Investigation of used PCM-integrated into building exterior walls for energy savings and optimization of PCM melting temperatures, *Constr. Build. Mater.*, 2023, **369**, 130601.

25 M. Wang, S. Liu, W. Gao and M. Zhou, Synthesis and characterization of Capric acid-Lauric acid/expanded vermiculite as a phase change composite for thermal energy storage, *J. Energy Storage*, 2024, **78**, 110091.

26 M. Amin, N. Putra, E. A. Kosasih, E. Prawiro, R. A. Luanto and T. Mahlia, Thermal properties of beeswax/graphene phase change material as energy storage for building applications, *Appl. Therm. Eng.*, 2017, **112**, 273–280.

27 S. A. Mohamed, F. A. Al-Sulaiman, N. I. Ibrahim, M. H. Zahir, A. Al-Ahmed, R. Saidur, B. Yılbaş and A. Sahin, A review on current status and challenges of inorganic phase change materials for thermal energy storage systems, *Renewable Sustainable Energy Rev.*, 2017, **70**, 1072–1089.

28 W. Sun, Z. Zhang, Z. Zhang, N. He, Q. Wei, L. Feng, Z. Wang, J. Wu, C. Liu and S. Fu, Photothermal phase change material microcapsules via cellulose nanocrystal and graphene oxide co-stabilized Pickering emulsion for solar and thermal energy storage, *Sci. China Mater.*, 2024, **67**, 3225–3235.

29 Q. Wei, W. Sun, Z. Zhang, G. Zhou and Z. Zhang, High thermal conductive and photothermal phase change material microcapsules via cellulose nanocrystal stabilized Pickering emulsion for solar harvesting and thermal energy storage, *Int. J. Biol. Macromol.*, 2025, **284**, 138162.

30 Y. Ding, L. Feng, Z. Zhang, S. Zhang, X. Zhang, Y. Li, X. Fang, X. Hu, X. Wang and K. C. Tam, Lignocellulose nanoparticles extracted from cattle dung as Pickering emulsifiers for microencapsulating phase change materials, *ACS Sustain. Chem. Eng.*, 2023, **11**, 14255–14266.

31 Z. Mo, P. Mo, M. Yi, Z. Hu, G. Tan, M. S. Selim, Y. Chen, X. Chen, Z. Hao and X. Wei, Ti_3C_2Tx@ polyvinyl alcohol foam-supported phase change materials with simultaneous enhanced thermal conductivity and solar-thermal conversion performance, *Sol. Energy Mater. Sol. Cells*, 2021, **219**, 110813.

32 Y. Chen, J. Chen, Z. Hao, M. S. Selim, J. Yu and X. Chen, Polyvinylpyrrolidone-bridged MXene skeleton constructed by photothermal assisted sacrificial template method for phase change materials with form stability and photothermal conversion, *Chem. Eng. J.*, 2023, **463**, 142375.

33 N. H. Mohamed, F. S. Soliman, H. El Maghraby and Y. Moustfa, Thermal conductivity enhancement of treated petroleum waxes, as phase change material, by α nano alumina: Energy storage, *Renewable Sustainable Energy Rev.*, 2017, **70**, 1052–1058.

34 R. Jacob and F. Bruno, Review on shell materials used in the encapsulation of phase change materials for high temperature thermal energy storage, *Renewable Sustainable Energy Rev.*, 2015, **48**, 79–87.

35 W. Su, J. Darkwa and G. Kokogiannakis, Review of solid–liquid phase change materials and their encapsulation technologies, *Renewable Sustainable Energy Rev.*, 2015, **48**, 373–391.

36 N. Zhang, Y. Yuan, Y. Du, X. Cao and Y. Yuan, Preparation and properties of palmitic-stearic acid eutectic mixture/expanded graphite composite as phase change material for energy storage, *Energy*, 2014, **78**, 950–956.

37 Y. Yang, C. Liu, Y. Shi, J. Hu, H. Chang and Y. He, A novel form-stable phase-change material with high enthalpy and long endurance for photo-thermal energy storage, *Bull. Mater. Sci.*, 2023, **46**, 146.

38 D. Zhou, J. Yuan, Y. Zhou and Y. Liu, Preparation and characterization of myristic acid/expanded graphite composite phase change materials for thermal energy storage, *Sci. Rep.*, 2020, **10**, 10889.

39 V. Srivastava and P. Mishra, CMOS compatible novel integration solution for broad range tunable photodetection using phase-change material based heterostructures, *Sci. Rep.*, 2020, **10**, 1–14.

40 Y. Yang, S. Xiong, J. Fu, Y. He, Y. Wu and Y. Xu, A novel form stable phase change material with comb-like cross-linked polyurethane as supporting skeleton, *Sci. Rep.*, 2023, **13**, 5243.

41 Y. Chen, Q. Zhang, X. Wen, H. Yin and J. Liu, A novel CNT encapsulated phase change material with enhanced thermal conductivity and photo-thermal conversion performance, *Sol. Energy Mater. Sol. Cells*, 2018, **184**, 82–90.

42 C. Li, B. Zhang, B. Xie, X. Zhao, J. Chen, Z. Chen and Y. Long, Stearic acid/expanded graphite as a composite phase change thermal energy storage material for tankless solar water heater, *Sustain. Cities Soc.*, 2019, **44**, 458–464.

43 X. Yang, Y. Yuan, N. Zhang, X. Cao and C. Liu, Preparation and properties of myristic–palmitic–stearic acid/expanded graphite composites as phase change materials for energy storage, *Sol. Energy*, 2014, **99**, 259–266.

44 R. Wen, Y. Liu, C. Yang, X. Zhu, Z. Huang, X. Zhang and W. Gao, Enhanced thermal properties of stearic acid/carbonized maize straw composite phase change material for thermal energy storage in buildings, *J. Energy Storage*, 2021, **36**, 102420.